Article

Anionic Charge Is Prioritized over Geometry in Aluminum and Magnesium Fluoride Transition State Analogs of Phosphoryl Transfer Enzymes

Nicola J. Baxter, G. Michael Blackburn, James P. Marston, Andrea M. Hounslow, Matthew J. Cliff, Wolfgang Bermel, Nicholas H. Williams, Florian Hollfelder, David E. Wemmer, and Jonathan P. Waltho

J. Am. Chem. Soc., **2008**, 130 (12), 3952-3958 • DOI: 10.1021/ja078000n

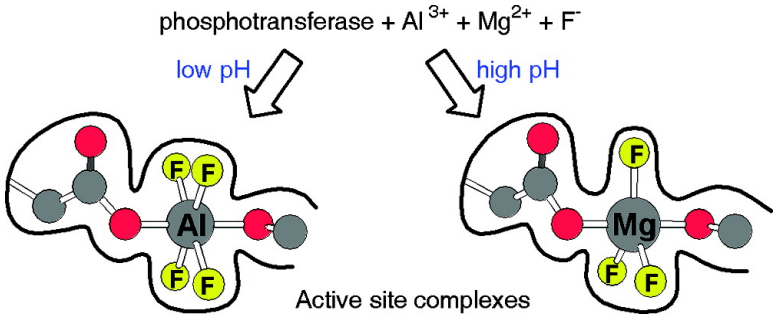

More About This Article

Additional resources and features associated with this article are available within the HTML version:

- Supporting Information
- Links to the 1 articles that cite this article, as of the time of this article download
- Access to high resolution figures
- Links to articles and content related to this article
- Copyright permission to reproduce figures and/or text from this article

View the Full Text HTML

J|A|C|S
ARTICLES
Published on Web 03/05/2008

Anionic Charge Is Prioritized over Geometry in Aluminum and Magnesium Fluoride Transition State Analogs of Phosphoryl Transfer Enzymes

Nicola J. Baxter,[†] G. Michael Blackburn,[‡] James P. Marston,[†] Andrea M. Hounslow,[†] Matthew J. Cliff,[†] Wolfgang Bermel,[§] Nicholas H. Williams,[‡] Florian Hollfelder,[||] David E. Wemmer,[+] and Jonathan P. Waltho*,[†]

Department of Molecular Biology and Biotechnology, University of Sheffield, Sheffield S10 2TN, United Kingdom, Centre of Chemical Biology, Department of Chemistry, University of Sheffield, Sheffield S3 7HF, United Kingdom, Bruker BioSpin GmbH, Siberstreifen 4, 76287 Rheinstetten, Germany, Department of Biochemistry, 80 Tennis Court Road, University of Cambridge, Cambridge CB2 1GA, United Kingdom, and Department of Chemistry, MC-1460, University of California, Berkeley, California 94720

Received October 18, 2007; E-mail: j.waltho@sheffield.ac.uk

Abstract: Phosphoryl transfer reactions are ubiquitous in biology and metal fluoride complexes have played a central role in structural approaches to understanding how they are catalyzed. In particular, numerous structures of AlF_x-containing complexes have been reported to be transition state analogs (TSAs). A survey of nucleotide kinases has proposed a correlation between the pH of the crystallization solution and the number of coordinated fluorides in the resulting aluminum fluoride TSA complexes formed. Enzyme ligands crystallized above pH 7.0 were attributed to AlF_3, whereas those crystallized at or below pH 7.0 were assigned as AlF_4^-. We use ^{19}F NMR to show that for β-phosphoglucomutase from *Lactococcus lactis*, the pH-switch in fluoride coordination does not derive from an AlF_4^- moiety converting into AlF_3. Instead, AlF_4^- is progressively replaced by MgF_3^- as the pH increases. Hence, the enzyme prioritizes anionic charge at the expense of preferred native trigonal geometry over a very broad range of pH. We demonstrate similar behavior for two phosphate transfer enzymes that represent typical biological phosphate transfer catalysts: an amino acid phosphatase, phosphoserine phosphatase from *Methanococcus jannaschii* and a nucleotide kinase, phosphoglycerate kinase from *Geobacillus stearothermophilus*. Finally, we establish that at near-physiological ratios of aluminum to magnesium, aluminum can dominate over magnesium in the enzyme-metal fluoride inhibitory TSA complexes, and hence is the more likely origin of some of the physiological effects of fluoride.

Introduction

The catalysis of phosphoryl transfer reactions ranks extremely highly in the range of rate accelerations achieved by enzymes. The spontaneous rate of hydrolysis of phosphate diesters ($t_{1/2}$ 3 $\times$ 10^7 years at 25 °C)[1] can be compared to an enzyme-catalyzed diesterase k_{cat} of 95 s^{-1} (*Staphylococcal* nuclease) giving a rate acceleration of 10^{17}, whereas cognate studies on phosphate monoester hydrolysis have estimated enzyme rate accelerations achieved by typical monoesterases in the region of 10^{21}.[2] A wide range of methodologies have been applied to characterize and rationalize such remarkably proficient catalysis.[3] Structural studies have contributed strongly to this effort, in particular with the advent of data based on transition state analogs (TSAs) in place of the scissile phosphate. Vanadates have been used in this role for some years[4] and, more recently, metal fluoride complexes have been introduced.[5] Beryllium fluoride complexes have provided good mimics of tetrahedral metastable phosphorylated species,[6] while aluminum fluoride (AlF_x) complexes[7]

[†] Department of Molecular Biology and Biotechnology, University of Sheffield.
[‡] Centre of Chemical Biology, Department of Chemistry, University of Sheffield.
[§] Bruker BioSpin GmbH.
[||] Department of Biochemistry, University of Cambridge.
[+] Department of Chemistry, University of California.

(1) Schroeder, G. K.; Lad, C.; Wyman, P.; Williams, N. H.; Wolfenden, R. *Proc. Natl. Acad. Sci. U.S.A.* **2006**, *103*, 4052−4055.
(2) Lad, C.; Williams, N. H.; Wolfenden, R. *Proc. Natl. Acad. Sci. U.S.A.* **2003**, *100*, 5607−5610.
(3) Cleland, W. W.; Hengge, A. C. *Chem. Rev.* **2006**, *106*, 3252−3278.
(4) Davies, D. R.; Hol, W. G. J. *FEBS Lett.* **2004**, *577*, 315−321.
(5) (a) Wittinghofer, A. *Curr. Biol.* **1997**, *7*, R682−R685. (b) Chabre, M. *Trends Biochem. Sci.* **1990**, *15*, 6−10. (c) Thompson, P. R.; Cole, P. A. *Proc. Natl. Acad. Sci. U.S.A.* **2001**, *98*, 8170−8171.
(6) (a) Cho, H.; Wang, W.; Kim, R.; Yokota, H.; Damo, S.; Kim, S.-H.; Wemmer, D.; Kustu, S.; Yan, D. *Proc. Natl. Acad. Sci. U.S.A.* **2001**, *98*, 8525−8530. (b) Kagawa, R.; Montgomery, M. G.; Braig, K.; Leslie, A. G. W.; Walker, J. E. *EMBO J.* **2004**, *23*, 2734−2744.
(7) (a) Rittinger, K.; Walker, P. A.; Eccleston, J. F.; Smerdon, S. J.; Gamblin, S. J. *Nature* **1997**, *389*, 758−762. (b) Scheffzek, K.; Ahmadian, M. R.; Kabsch, W.; Wiesmüller, L.; Lautwein, A.; Schmitz, F.; Wittinghofer, A. *Science* **1997**, *277*, 333−338. (c) Xu, Y.-W.; Morera, S.; Janin, J.; Cherfils, J. *Proc. Natl. Acad. Sci. U.S.A.* **1997**, *94*, 3579−3583. (d) Nassar, N.; Hoffman, G. R.; Manor, D.; Clardy, J. C.; Cerione, R. A. *Nat. Struct. Biol.* **1998**, *5*, 1047−1052. (e) Menz, R. I.; Walker, J. E.; Leslie, A. G. W. *Cell* **2001**, *106*, 331−341.

 10.1021/ja078000n CCC: $40.75

have been used widely as TSAs for the phosphoryl transfer reaction, and are the closest models obtained so far for the catalytic transition state.

Numerous structures of AlF_x-containing TSA complexes of phosphoryl transfer enzymes have been reported and a survey of nucleotide kinases[8] proposed a correlation between the pH of the crystallization solution and the number of coordinated fluorides in the TSA complexes formed. Where the atomic resolution was adequate, enzymes crystallized in the presence of Mg^{2+} above pH 7.0 were observed to contain a central trigonal planar moiety, attributed to AlF_3, while those crystallized at or below pH 7.0, with two exceptions, contained a central square planar moiety, attributed to AlF_4^-. The reason for the switch in coordination with pH was not resolved, but was proposed to result either from a change in ionization state within the complex, suggested to be the β-phosphate group of the nucleotide, or from the pH-dependent switch between different coordination states observed for aluminum hydroxyls and fluorides in solution.[8] However, neither proposal accounts fully for all the data. For example, the observation of such a switch from a square planar moiety to a trigonal planar moiety in a phosphoryl transfer TSA complex has not been limited to nucleotide kinases and nucleotide phosphatases—the crystal structure of phosphoserine phosphatase with AlF_x species revealed an approximately equal population of both square planar and trigonal planar complexes within the enzyme active site.[9]

Our recent analysis by ^{19}F NMR of a TSA complex containing MgF_3^- in the active site of β-phosphoglucomutase from *Lactococcus lactis* (β-PGM, EC 5.4.2.6, 25 kDa)[10] has provided a new opportunity to interrogate the geometric switches in these TSAs of phosphoryl transfer. The phosphoryl transfer reaction catalyzed by phosphorylated β-PGM in the presence of magnesium ions involves the reversible interconversion of β-glucose 1-phosphate and β-glucose 6-phosphate (G6P) via a β-glucose 1,6-bisphosphate intermediate.[11] The reaction is inhibited by fluoride with an IC_{50} in the low millimolar range[10] owing to the formation of a five-coordinate magnesium atom with three equatorial fluorine atoms plus two apical oxygen atoms donated by the C-1 hydroxyl of G6P and OD1 of Asp8.[10,12] This complex is termed here PGM-MgF_3-TSA.

Here, we show that the pH-switch in fluoride coordination derives not from an AlF_4^- moiety converting into AlF_3 but rather that AlF_4^- is progressively replaced by MgF_3^- as the pH increases. Hence, the near-transition state complex prioritizes anionic charge character over a very broad range of pH at the expense of geometry (trigonal bipyramidal versus octahedral). Furthermore, many of the physiological effects of elevated levels of fluoride have been associated with enzymes for which aluminum fluoride species could act as inhibitors.[13] However, the demonstration of stable TSA complexes containing magnesium fluoride for β-PGM[10] and for RhoA.GDP/RhoGAP,[14] brings into question whether fluoride inhibition of physiologically important enzymes has an alternative origin in vivo where the more abundant Mg^{2+} ions might out-compete Al^{3+} ions in TSA complexes. Given the accessibility of β-PGM to ^{19}F NMR observation of metal fluoride complex species, we have also used this enzyme to study the competition between the aluminum fluoride and magnesium fluoride TSA species.

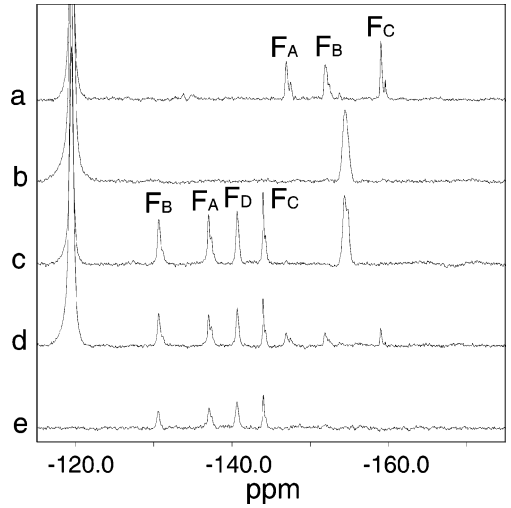

Figure 1. ^{19}F NMR spectra of PGM-MgF_3-TSA and PGM-AlF_4-TSA complexes at pH 7.2. (a) PGM-MgF_3-TSA showing MgF_3^- ($F_A = -147$, $F_B = -152$, $F_C = -159$ ppm) and free F^- at -119 ppm. (b) $(H_2O)_2AlF_4^-$ and $(HO)AlF_3^-$ species (AlF_x species) at -154 ppm in fast exchange[15] for the components of PGM-AlF_4-TSA (5 mM $MgCl_2$, 10 mM NH_4F and 1 mM $AlCl_3$ in 50 mM K^+ HEPES buffer) in the absence of β-PGM. (c) PGM-AlF_4-TSA showing AlF_4^- ($F_B = -130$, $F_A = -137$, $F_D = -141$, $F_C = -144$ ppm) and AlF_x at -154 ppm. (d) The addition of substoichiometric Al^{3+} to PGM-MgF_3-TSA results in a mixture of PGM-MgF_3-TSA and PGM-AlF_4-TSA complexes. (e) PGM-MgF_3-TSA cannot be recovered from PGM-AlF_4-TSA even in the presence of 500 mM $MgCl_2$ and 100 mM NH_4F. Excess Mg^{2+} in solution associates with free F^- resulting in the peak at -119 ppm being broadened beyond detection.

Results

PGM-MgF_3-TSA Is Converted into an AlF_4^- Containing TSA by the Addition of Al^{3+}. The ^{19}F NMR spectrum of PGM-MgF_3-TSA shows three ^{19}F resonances ($F_A = -147$, $F_B = -152$, $F_C = -159$ ppm), present in a 1:1:1 ratio that is also stoichiometric with β-PGM concentration (Figure 1a), as previously reported.[10] The presence of well-resolved peaks indicates that there are three distinct sites for fluoride binding in the complex, and each is occupied with a lifetime well in excess of 10 s, as determined by the lack of saturation transfer between ^{19}F resonances following selective irradiation of each resonance.[10] Eleven NOEs from the three fluorides to the backbone amide protons of β-PGM define the MgF_3^- moiety stabilized in the active site as having trigonal planar geometry.[10] On addition of Al^{3+} to PGM-MgF_3-TSA, four new ^{19}F resonances ($F_B = -130$, $F_A = -137$, $F_D = -141$, $F_C = -144$ ppm) appear simultaneously with a 1:1:1:1 ratio (Figure 1c) consistent with the formation of a TSA complex comprising

(8) Schlichting, I.; Reinstein, J. *Nat. Struct. Biol.* **1999**, *6*, 721−723.
(9) Wang, W.; Cho, H. S.; Kim, R.; Jancarik, J.; Yokota, H.; Nguye, H. H.; Grigoriev, I. V.; Wemmer, D. E.; Kim, S.-H. *J. Mol. Biol.* **2002**, *319*, 421−431.
(10) Baxter, N. J.; Olguin, L. F.; Goličnik, M.; Feng, G.; Hounslow, A. M.; Bermel, W.; Blackburn, G. M.; Hollfelder, F.; Waltho, J. P.; Williams, N. H. *Proc. Natl. Acad. Sci. U.S.A.* **2006**, *103*, 14732−14737.
(11) (a) Qian, N.; Stanley, G. A.; Hahn-Hägerdal, B.; Rådström, P. *J. Bacteriol.* **1994**, *176*, 5304−5311. (b) Qian, N.; Stanley, G. A.; Bunte, A.; Rådström, P. *Microbiol.* **1997**, *143*, 855−865.
(12) Blackburn, G. M.; Williams, N. H.; Gamblin, S. J.; Smerdon, S. J. *Science* **2003**, *301*, 1184c.
(13) Li, L. *Crit. Rev. Oral Biol. Med.* **2003**, *14*, 100−114.
(14) (a) Graham, D. L.; Eccleston, J. F.; Chung, C.-W.; Lowe, P. N. *Biochemistry* **1999**, *38*, 14981−14987. (b) Graham, D. L.; Lowe, P. N.; Grime, G. W.; Marsh, M.; Rittinger, K.; Smerdon, S. J.; Gamblin, S. J.; Eccleston, J. F. *Chem. Biol.* **2002**, *9*, 375−381.
(15) (a) Martin, R. B. *Biochem. Biophys. Res. Commun.* **1988**, *155*, 1194−1200. (b) Bodor, A.; Tóth, I.; Banyai, I.; Szabo, A.; Hefter, G. T. *Inorg. Chem.* **2000**, *39*, 2530−2537.

AlF_4^-, G6P and β-PGM (PGM-AlF_4-TSA). There is a concomitant loss of the three peaks arising from PGM-MgF_3-TSA. With a sub-stoichiometric addition of Al^{3+} to PGM-MgF_3-TSA (Figure 1d), a mixture of both PGM-MgF_3-TSA and PGM-AlF_4-TSA exists with the proportion of PGM-AlF_4-TSA being determined by the amount of Al^{3+} added. With an above stoichiometric addition of Al^{3+}, no ^{19}F resonances for the MgF_3^- moiety are observed. The concerted simultaneous appearance and disappearance of separate sets of ^{19}F resonances for PGM-AlF_4-TSA and for PGM-MgF_3-TSA respectively, indicate that assembly and disassembly of the TSA components in the β-PGM active site occurs without significant population of intermediates. Additionally, and as for PGM-MgF_3-TSA, the four fluoride sites of PGM-AlF_4-TSA are distinct, are not rotationally averaged and are occupied with a lifetime well in excess of 10 s.

The PGM-AlF_4-TSA Complex Is Dominant at Physiological Mg^{2+}/Al^{3+} Ratios. In order to test whether the physiological consequences of elevated fluoride concentrations are more likely to result from inhibition through the formation of PGM-AlF_4-TSA or PGM-MgF_3-TSA, we explored the ability of Mg^{2+} to displace the PGM-AlF_4-TSA complex. The physiological concentrations of Al^{3+} appear not to be strongly regulated within cells, and basal concentrations tend to reflect serum concentrations, which in turn reflect the local water supply. This places cellular Al^{3+} concentrations in the range 1−10 μM, while Mg^{2+} concentrations tend to fall in the range 1−10 mM.[16] Allowing for the limitations of recording ^{19}F NMR spectra of β-PGM at elevated Mg^{2+} concentrations, it was possible to test the competition between the two metal fluoride complexes in the presence of an excess of Mg^{2+} over Al^{3+} up to 500-fold. Under these conditions, PGM-AlF_4-TSA remains the only species measurably populated (Figure 1e), indicating that at least in the case of β-PGM, PGM-AlF_4-TSA is the dominant complex at 25 °C and neutral pH, even accounting for the large molar excess of Mg^{2+} present in cells.

Chemical Shift Differences between PGM-MgF_3-TSA and PGM-AlF_4-TSA Map to Active Site Loops. The backbone amide proton and nitrogen chemical shifts obtained from the resonance assignment procedure were used to obtain chemical shift changes ($\Delta\delta$) on switching from PGM-MgF_3-TSA to PGM-AlF_4-TSA (Figure 2). Overall, the observed changes are small, but moderately widespread. The lack of chemical shift changes for most of the residues of β-PGM indicates that the backbone scaffolding regions for PGM-AlF_4-TSA remain very similar to the X-ray structure determined for PGM-MgF_3-TSA[17] (PDB accession code 1O08). Five segments of residues that exhibit measurable $\Delta\delta$ (F7-H20, K45-S52, A113-N118, D137-K145 and L168-A177) map to regions of β-PGM directly involved in substrate and metal fluoride binding (Figure 2). Two further segments with measurable $\Delta\delta$ (D149-H156 and S205-T208) are adjacent to the catalytic site. The observed effects are small enough to arise from subtle alterations in bond lengths and angles of the hydrogen bond network demanded as a square planar AlF_4^- moiety replaces the trigonal planar MgF_3^- moiety. The two hinge regions between the cap and the core domains (T14-D15 and V92-Y93)[18] also show small $\Delta\delta$, indicating that the two metal fluoride complexes are adopting similar closed conformations. Hence, there is no evidence for substantial conformational change. Using TALOS,[19] ϕ and ψ dihedral angles were predicted from the chemical shift values obtained for PGM-MgF_3-TSA and PGM-AlF_4-TSA and were compared to the dihedral angles calculated from the PGM-MgF_3-TSA structure. For both PGM-MgF_3-TSA and PGM-AlF_4-TSA, the predicted values of ϕ and ψ for each residue were equivalent to those of the crystal structure within the errors of the TALOS calculation and no systematic correlation exists between changes in dihedral angle values and large $\Delta\delta$.

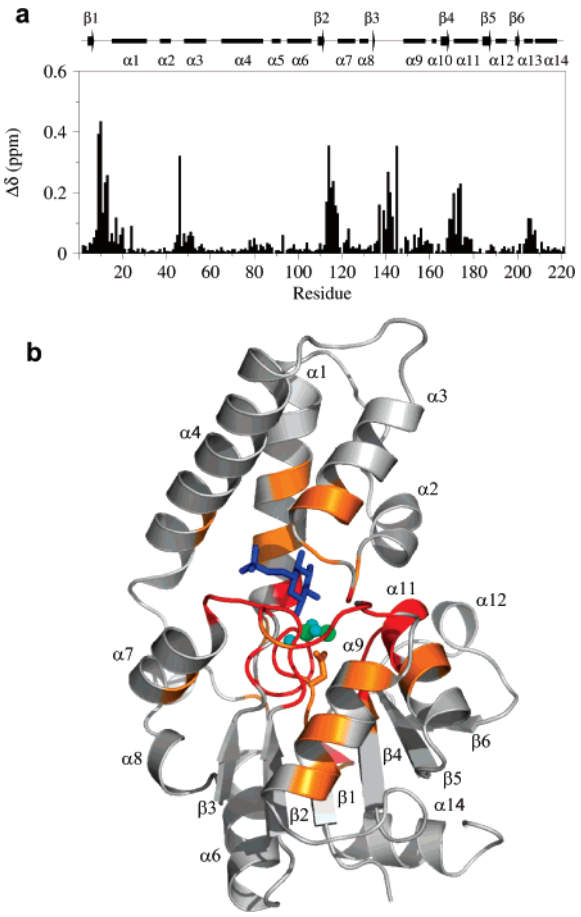

Figure 2. (a) Histogram of the residue specific chemical shift changes on switching from PGM-MgF_3-TSA to PGM-AlF_4-TSA. Absolute chemical shift changes ($\Delta\delta$) were calculated using the following equation: $\Delta\delta = [(\delta_{HN}MgF_3\text{-TSA} - \delta_{HN}AlF_4\text{-TSA})^2 + (C(\delta_N MgF_3\text{-TSA} - \delta_N AlF_4\text{-TSA}))^2]^{1/2}$, where δ_{HN} = chemical shift of the backbone amide proton, δ_N = chemical shift of the backbone amide nitrogen and $C = 0.12$ for the rescaling of the δ_N values. The residue segments that exhibit significant $\Delta\delta$ are involved directly in substrate and metal fluoride binding (F7-H20, K45-S52, A113-N118, D137-K145, and L168-A177) or are more peripheral to the catalytic site (D149-H156 and S205-T208). The arrows and bars represent β-strands and α-helices labeled sequentially. (b) The PGM-MgF_3-TSA complex with residues colored according to $\Delta\delta$. Residues with large $\Delta\delta$ values ($\Delta\delta > 0.1$ ppm) are colored red and map almost exclusively to the active site loops, and residues with smaller $\Delta\delta$ values (0.1 ppm $\geq \Delta\delta > 0.05$ ppm) are colored orange. The side chain of the catalytic residue Asp8 is shown as a wireframe and G6P is colored blue. The two Mg^{2+} ions and the three F^- ions in the active site are depicted as green and cyan spheres, respectively, with the trigonal planar MgF_3^- moiety positioned to the left and the bound Mg^{2+} cofactor required for catalytic activity positioned to the right.

(16) Martin, R. B. *Clin. Chem.* **1986**, *32*, 1797−1806.
(17) Lahiri, S. D.; Zhang, G.; Dunaway-Mariano, D.; Allen, K. N. *Science* **2003**, *299*, 2067−2071.
(18) Lahiri, S. D.; Zhang, G.; Dunaway-Mariano, D.; Allen, K. N. *Biochemistry* **2002**, *41*, 8351−8359.
(19) Cornilescu, G.; Delaglio, F.; Bax, A. *J. Biomol. NMR* **1999**, *13*, 289−302.

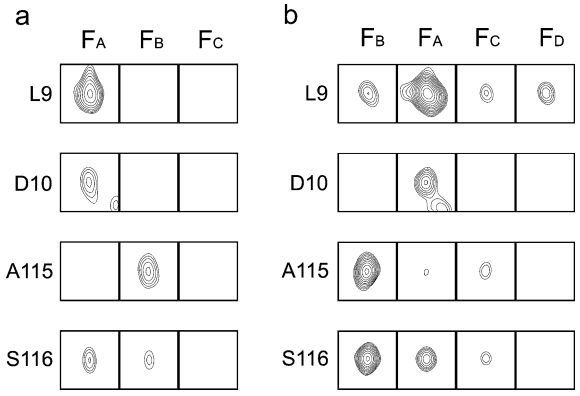

Figure 3. (a) Regions of the 2D frequency selective $\{^{19}F\}^{1}H,^{15}N$-HSQC NOE difference spectra of the PGM-MgF_3-TSA complex showing NOEs between fluorides F_A, F_B, and F_C of the MgF_3^- moiety and four backbone amide protons from residues L9, D10, A115, and S116 of β-PGM. For each region, the HN axis (*x*-axis) range is 0.2 ppm and the N axis (*y*-axis) range is 1.0 ppm. (b) Regions of the 2D frequency selective $\{^{19}F\}^{1}H,^{15}N$-HSQC NOE difference spectra of the PGM-AlF_4-TSA complex showing NOEs between fluorides F_B, F_A, F_D, and F_C of the AlF_4^- moiety and four backbone amide protons from residues L9, D10, A115, and S116 of β-PGM. For each region, the HN axis (*x*-axis) range is 0.2 ppm and the N axis (*y*-axis) range is 0.8 ppm.

Assignment of NOEs between Fluoride and Amide Protons in PGM-AlF_4-TSA. Selective irradiation of each of the four fluoride resonances in the PGM-AlF_4-TSA complex established the existence of different $\{^{19}F\}^{1}H$-NOE distributions between the fluorides and the backbone amide protons of β-PGM. Resolution of the amide proton resonances involved in these NOEs was achieved using selective $\{^{19}F\}^{1}H,^{15}N$-HSQC NOE difference spectra[10] of $^{2}H,^{15}N$-labeled β-PGM in the PGM-AlF_4-TSA complex (Figure 3). Identification of the amide proton partners for a total of 38 $\{^{19}F\}^{1}H$-NOEs was accomplished following the assignment of the $^{1}H,^{15}N$ peaks in a 2D $^{1}H,^{15}N$-TROSY spectrum. The 38 NOEs identified were employed as restraints to move four fluorides into the closed conformation of β-PGM[17] (PDB accession code 1O08) from random starting coordinates using standard solution structure determination procedures within the program CNS.[20] The small changes in chemical shift observed and the TALOS analysis performed indicate that the backbone coordinates of β-PGM in the crystal structure of the PGM-MgF_3-TSA complex are appropriate for the NOE directed docking of four fluorides into the active site and generation of the PGM-AlF_4-TSA structure.

The resulting positional distribution of the fluorides confirmed that the PGM-AlF_4-TSA complex consists of four fluorides coordinated in a square planar arrangement around a central Al^{3+} positioned in the active site (Figure 4). Compared with the PGM-MgF_3-TSA complex, fluoride F_A occupies a similar position in both structures and is hydrogen bonded by L9 and D10 backbone amide protons and the side chain hydroxyl group of S114. Fluoride F_B is located closer to the backbone NH group of S116 in the PGM-AlF_4-TSA structure. Fluoride F_C, which is diametrically opposite fluoride F_B in the square planar arrangement, still fulfils the role of the bridging fluoride to the catalytic Mg^{2+} ion and fluoride F_D is positioned diametrically opposite fluoride F_A.

(20) Brunger, A. T.; Adams, P. D.; Clore, G. M.; Delano, W. L.; Gros, P.; Grosse-Kunstleve, R. W.; Jiang, J.-S.; Kuszewski, J.; Nilges, M.; Pannu, N. S.; Read, R. J.; Rice, L. M.; Simonson, T.; Warren, G. L. *Acta. Crystallogr.* **1998**, *D54*, 905−921.

PGM-AlF_4-TSA Spontaneously Converts into PGM-MgF_3-TSA at High pH. To address how solution pH influences the number of coordinated fluorides in the β-PGM aluminum fluoride TSA complexes, ^{19}F NMR spectra were recorded for β-PGM in the presence of Al^{3+}, Mg^{2+}, G6P, and F^- over the pH range 6.6 − 9.4 (Figure 5). The peak at −154 ppm corresponds to resonances of $(H_2O)_2AlF_4^-$ and $(HO)AlF_3^-$ (AlF_x species), which are in fast exchange and are unresolved under these conditions.[15] The signal for free AlF_x disappears by pH 7.8, as aluminum hydroxide species become dominant. The remaining peaks show that PGM-AlF_4-TSA is the only species detectable in solution below pH 8.2. Between pH 8.6 and 9.4, the population of PGM-AlF_4-TSA gradually decreases until its four ^{19}F peaks become undetectable. There are no chemical shift changes for these resonances, indicating that the charge distribution within the active site is retained throughout. The decrease in PGM-AlF_4-TSA resonances is exactly mirrored by an increase in the population of a second species characterized by three distinct ^{19}F resonances (−147, −152, −159 ppm), present in a 1:1:1 ratio, which becomes the exclusive complex observable in solution at pH 9.4. The three resonances of the second species are identical in chemical shift, intensity and line shape to those present in equivalent samples prepared in the absence of Al^{3+}. Thus, they result from the population of the PGM-MgF_3-TSA complex.

It is noteworthy that chemical shift changes also do not occur for ^{19}F resonances of PGM-MgF_3-TSA over the entire pH range tested. This indicates that there is no change in protonation state of any titratable residue and hence the charge distribution within the active site is retained throughout (Figure 5). The identity of the second species populated at high pH is further supported by equilibrating PGM-AlF_4-TSA at pH 9.4 before reducing it to pH 7.0. Here, a mixture of PGM-AlF_4-TSA and the second species (PGM-MgF_3-TSA) coexist at pH 7.0, since there is insufficient Al^{3+} available for the exclusive formation of PGM-AlF_4-TSA. At basic pH values (with 10 mM F^-) Al^{3+} irreversibly precipitated, most likely as $Al(OH)_3$ and $Al(OH)_2H_2PO_4$ species.[16,21] Inorganic phosphate (1−5 mM) was present in the NMR solutions as a result of the hydrolysis of phosphorylated β-PGM formed during the uninhibited reaction with G6P. Further addition of Al^{3+} to the mixture of PGM-MgF_3-TSA and PGM-AlF_4-TSA complexes restored PGM-AlF_4-TSA and free AlF_x as the only species observable in solution.

No Evidence for AlF_3 Containing TSA Complexes in Other Phosphoryl Transfer Enzymes. In order to establish whether the absence of an AlF_3 containing TSA complex was a particular (and unusual) property of β-PGM, we examined the aluminum fluoride TSA complexes of phosphoserine phosphatase from *M. jannaschii* (PSP, EC 3.1.3.3, 24 kDa). PSP was chosen following a report that both AlF_4^- containing TSA and AlF_3 containing TSA complexes were present simultaneously in crystals of PSP grown at pH 7.5.[9] At pH 6.4, 1D ^{19}F NMR spectra showed that the predominantly populated species was PSP-AlF_4-TSA with four ^{19}F resonances present (F_1 = −133, F_2 = −134, F_3 = −141, and F_C = −149 ppm) (Figure 6). The resonance at −149 ppm was assigned as the bridging fluoride to the catalytic Mg^{2+} ion on account of its narrower line width and upfield chemical shift. At pH values above 8.8,

(21) Strunecká, A.; Strunecký, O.; Patočka, *J. Physiol. Res.* **2002**, *51*, 557−564.

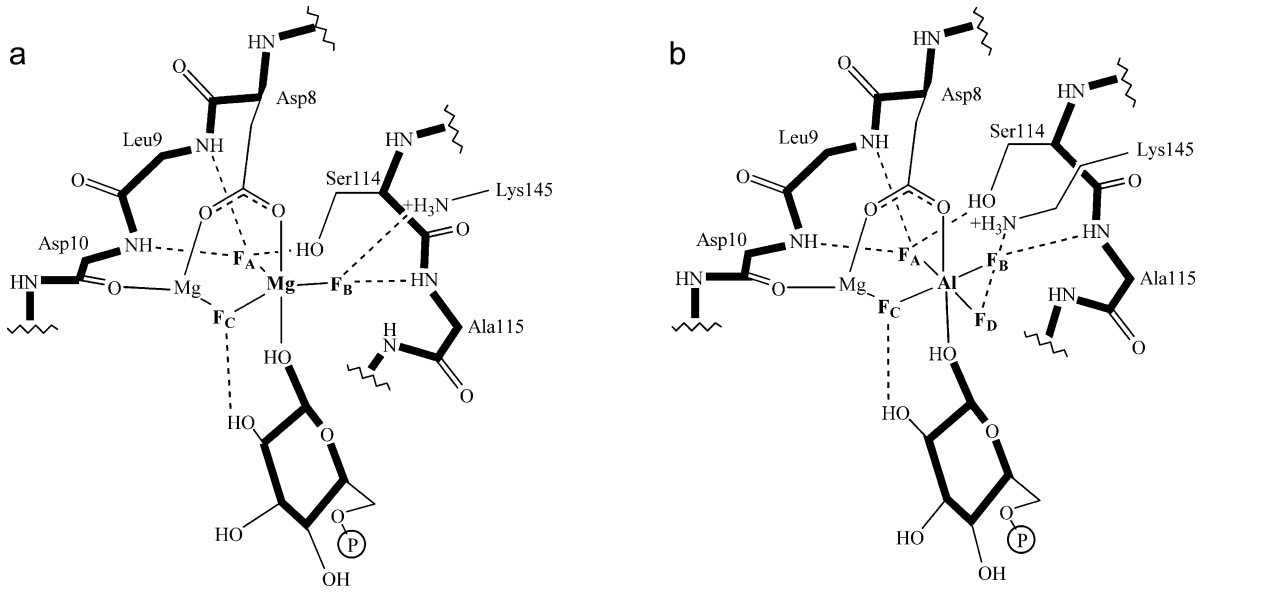

Figure 4. Structural comparison of the β-PGM metal fluoride TSAs (a) PGM-MgF_3-TSA.[10] (b) PGM-AlF_4-TSA. The four enzyme-bound fluorides were docked according to the 38 NOEs to the backbone amide protons. The protein structure[17] (PDB accession code 1O08) was used as a template and the fluorides were docked as described previously.[10]

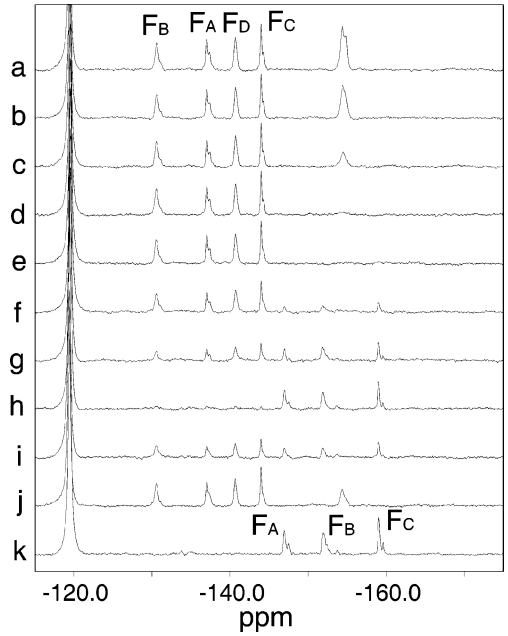

Figure 5. pH titration of the PGM-AlF_4-TSA complex monitored by ^{19}F NMR. (a) pH 6.6 and $F_B = -130$, $F_A = -137$, $F_D = -141$, and $F_C = -144$ ppm (b) pH 7.0 (c) pH 7.4 (d) pH 7.8 (e) pH 8.2 (f) pH 8.6 (g) pH 9.0 (h) pH 9.4 (i) pH 7.0 (j) following addition of a further 0.5 mM $AlCl_3$ at pH 7.0 (k) PGM-MgF_3-TSA at pH 7.2 and $F_A = -147$, $F_B = -152$, and $F_C = -159$ ppm.

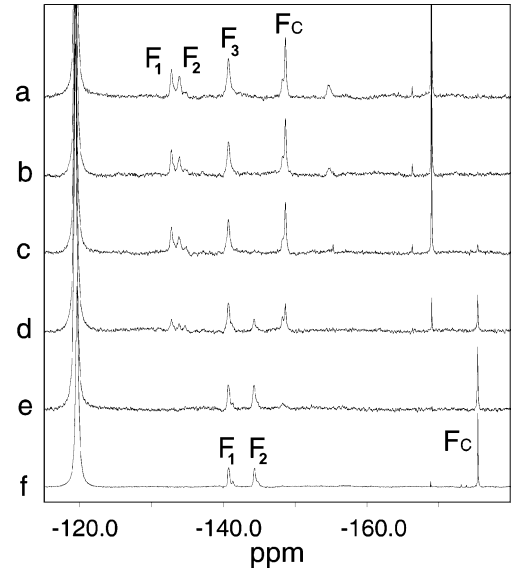

Figure 6. pH titration of the PSP-AlF_4-TSA complex monitored by ^{19}F NMR. (a) pH 6.4 and $F_1 = -133$, $F_2 = -134$, $F_3 = -141$, and $F_C = -149$ ppm (b) pH 7.2 (c) pH 8.0 (d) pH 8.8 (e) pH 9.2 (f) PSP-MgF_3-TSA at pH 6.4 and $F_1 = -141$, $F_2 = -144$, and $F_C = -176$ ppm. The ^{19}F resonances at -154 ppm correspond to unbound AlF_x species and those between -160 and -170 ppm correspond to other non-proteinaceous metal fluorides.

a trifluoride species became observable with three ^{19}F resonances ($F_1 = -141$, $F_2 = -144$, and $F_C = -176$ ppm) and by pH 9.2 the trifluoride became the only species detectable. As in the case of β-PGM, the trifluoride species was confirmed to be PSP-MgF_3-TSA, and not PSP-AlF_3-TSA, by comparison of ^{19}F chemical shifts to equivalent complexes prepared with the exclusion of Al^{3+}. As noted previously, the chemical shifts of the ^{19}F resonances of both PSP-MgF_3-TSA and PSP-AlF_4-TSA complexes were not affected markedly by pH, indicating that the environment of the active site was again strongly resistant to change.

Finally, to establish whether nucleotide kinases show similar behavior to these non-nucleotide kinases, we repeated the pH titration with phosphoglycerate kinase from *G. stearothermophilus* (PGK, EC 2.7.2.3, 43 kDa). For PGK, a population of the PGK-MgF_3-TSA complex containing 3-phosphoglycerate and ADP was not detectable in solution, implying that the hydrogen bond donors in the active site are unable to stabilize the formation of the MgF_3^- moiety. However, on addition of Al^{3+} to the solution detailed above, a PGK-AlF_4-TSA complex was formed with four ^{19}F resonances ($F_1 = -136$, $F_2 = -139$, $F_3 = -142$, and $F_C = -147$ ppm) (Figure 7). The resonance at -147 ppm was assigned as for PSP to the bridging fluoride to the catalytic Mg^{2+} ion. On raising the pH to 8.4, the ^{19}F

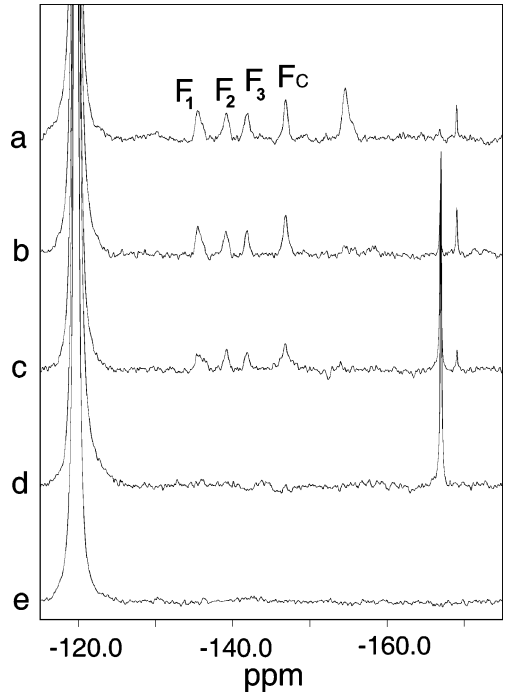

Figure 7. pH titration of the PGK-AlF_4-TSA complex monitored by ^{19}F NMR. (a) pH 7.6 and $F_1 = -136$, $F_2 = -139$, $F_3 = -142$, and $F_C = -147$ ppm (b) pH 8.0 (c) pH 8.4 (d) pH 8.8 (e) putative PGK-MgF_3-TSA at pH 7.6. The ^{19}F resonances at -154 ppm correspond to unbound AlF_x species and those between -160 and -170 ppm correspond to other non-proteinaceous metal fluorides.

resonances of the PGK-AlF_4-TSA complex did not change chemical shift significantly, but a decrease in intensity occurs between pH 8.0 and 8.4, similarly to the behavior of PGM-AlF_4-TSA and PSP-AlF_4-TSA complexes. Again, no evidence of a PGK-AlF_3-TSA complex was found.

Discussion

As observed for other phosphoryl transfer enzymes, the addition of Al^{3+} and fluoride to β-PGM in the presence of substrate (G6P) leads to the formation of a closed protein conformation around a metal fluoride TSA complex. The NMR spectra clearly establish that, in this case, the metal fluoride moiety is AlF_4^-. The protein conformation determined for the PGM-MgF_3-TSA is largely retained, except for the expected change from a trigonal planar to a square planar arrangement of the metal fluoride moiety, as observed for RhoA.GDP/Rho.GAP metal fluoride TSA complexes.[7a,14b] When treated equivalently, PSP and PGK also make closed TSA complexes containing AlF_4^-. Despite the difference in AlF_4^- geometry from that of the transferring phosphoryl group, the fluorides do not show rotational averaging, i.e., their positions are fixed for times in excess of seconds. Hence the individual fluorides are held tightly. While either of the PGM-MgF_3-TSA or PGM-AlF_4-TSA complexes can be the more populated species in solution under appropriate conditions, the PGM-MgF_3-TSA complex cannot be detected in the presence of stoichiometric levels of Al^{3+} even when Mg^{2+} is in a molar excess of 500:1. Hence, it is more likely that any physiological effects of enzyme inhibition by metal fluorides are the result of aluminum fluoride species.

The above results could be interpreted as the active site of β-PGM being better suited to the square planar arrangement of AlF_4^- rather than to the trigonal planar arrangement of MgF_3^-. Monomeric metaphosphate, PO_3^-, is both trigonal and anionic, and MgF_3^- is an isoelectronic and isosteric analog. MgF_3^- has a formal negative charge as has AlF_4^-, but its trigonal geometry is close to that ascribed to AlF_3 in protein complexes.[8] However, this is not established by the data, owing to the differences in both the metal bond strengths to the apical ligands and the availability of these species in aqueous solution. For example, AlF_4^- is readily observed in solution in the absence of enzyme (Figure 1) making it a significant AlF_x species at a fluoride concentration of 10 mM.[22] By contrast, MgF_3^- is not observable (MgF^+ is the dominant magnesium fluoride species at 278 K)[10] and conservative estimates from the formation constants for MgF^+ ($\beta_1 = 50\ M^{-1}$) and MgF_2 ($\beta_2 < 1.6 \times 10^3\ M^{-2}$)[23] and an approximate value of $\beta_3 < 5 \times 10^4\ M^{-3}$, place the concentration of MgF_3^- to be $<80\ \mu M$ under the conditions used here.

For both PGM-MgF_3-TSA and PGM-AlF_4-TSA complexes, the environment in which the metal fluoride is bonded is highly resilient to changes in pH. ^{19}F NMR resonances are extremely sensitive to perturbations in the environment of the ^{19}F nuclei, yet the fluoride chemical shifts are constant throughout the pH range examined. In contrast to the previous view that the proposed AlF_4 to AlF_3 switch[8] may result from the active site of some phosphoryl transfer enzymes having to accommodate moieties with pK_a's close to neutrality, in the cases of β-PGM, PSP, and PGK the charge distributions within the TSA complex active sites are not influenced by ionizations over a very broad pH range. Hence, the observed switch in metal fluoride geometry from square planar to trigonal planar with increasing pH arises from a completely different source. As the pH is increased, the geometry of aqueous aluminum fluoride species changes from octahedral aluminum fluoride (and aluminum fluoride/hydroxide mixed species) to tetrahedral aluminum hydroxide resulting from the displacement of fluoride ions by the cooperative nature of hydroxide ion binding.[15a,16,24] This causes the concentration of aluminum fluoride to fall below that of the enzyme, allowing the formation of a MgF_3^- transition state analog complex in the active site. Here, we show that the pH-switch in fluoride coordination derives not from an AlF_4^- moiety converting into AlF_3 but rather that AlF_4^- is progressively replaced by MgF_3^- as the pH increases. These observations reinforce two conclusions. First, the charge on the metal fluoride species dominates over its geometry in determining the preferred mode of binding since AlF_4^- out-competes AlF_3. Second, there is no evidence for any population of AlF_3 containing transition state analogs for these three enzymes. Therefore, it follows[14a] that several, if not a majority, of the high-pH AlF_3 transition state analog complexes reported for nucleotide kinases, should be treated with caution.

Materials and Methods

NMR Methods. Unlabeled, ^2H,^{15}N-labeled and ^2H,^{13}C,^{15}N-labeled β-PGM was expressed and purified as detailed previously.[10] The PGM-MgF_3-TSA samples for NMR analysis (600 μL) contained 0.5 mM β-PGM, 10 mM G6P, 5 mM $MgCl_2$, 10 mM NH_4F, 2 mM NaN_3 in 50 mM K^+ HEPES buffer (pH 7.2) and 15% v/v D_2O. The PGM-AlF_4-TSA samples were prepared by adding $AlCl_3$ to a concentration of <3 mM to the PGM-MgF_3-TSA samples defined above. Uniformly ^{15}N,^{13}C-

(22) Hefter, G.; Bodor, A.; Tóth, I. *Aust. J. Chem.* **2000**, *53*, 625−626.
(23) Fovet, Y.; Gal, J.-Y. *Talanta* **2000**, *53*, 617−626.
(24) Martin, R. B. *Coord. Chem. Rev.* **1996**, *141*, 23−32.

labeled PSP was expressed and purified as detailed previously.[9] The PSP-MgF_3-TSA sample for the NMR experiments (200 μL in a Shigemi tube) contained 0.5 mM PSP, 10 mM $MgCl_2$, 6 mM NH_4F, 1 mM NaN_3, 2 mM TCEP, 0.1 mM EDTA, and 10% v/v D_2O at pH 6.4. The PSP-AlF_4-TSA sample was prepared by adding 3 mM $AlCl_3$ to the PSP-MgF_3-TSA sample detailed above. Uniformly ^{15}N-labeled PGK was expressed and purified as detailed previously.[25] The putative PGK-MgF_3-TSA sample for the NMR experiments (500 μL) contained 0.25 mM PGK, 10 mM 3-phosphoglycerate, 5 mM ADP, 5 mM $MgCl_2$, 10 mM NH_4F, 1 mM NaN_3 2.5 mM DTT in 50 mM TEA buffer (pH 7.6) and 10% v/v D_2O. The PGK-AlF_4-TSA sample was prepared by adding 1 mM $AlCl_3$ to the PGK-MgF_3-TSA sample detailed above.

Backbone resonance assignments (HN, N, C^{β}, and C′) for PGM-AlF_4-TSA (with 1 mM ^{2}H,^{13}C,^{15}N-labeled β-PGM) were obtained by comparison with PGM-MgF_3-TSA backbone resonance assignments using data from 2D ^{15}N-TROSY, 3D TROSY HN(COCA)CB and 3D TROSY HNCO spectra acquired on a Bruker Avance 600 MHz spectrometer equipped with a 5-mm ^{1}H/^{15}N/^{13}C/^{2}H cryoprobe and pulse-field z-gradients. The data were acquired, processed, and analyzed as previously detailed.[10,25] The 1D ^{19}F NMR spectra were recorded on a Bruker Avance 500 MHz spectrometer equipped with a 5 mm dual ^{1}H/^{19}F probe. Typically, 1500 transients were acquired over a spectral width of 100 ppm with the carrier frequency set to −140 ppm. The 2D frequency selective {^{19}F}^{1}H,^{15}N-HSQC NOE difference spectra of PGM-AlF_4-TSA (sample prepared as above with 1 mM ^{2}H,^{15}N-labeled β-PGM, 14 mM G6P and 2 mM $AlCl_3$) were acquired on a Bruker Avance 600 MHz spectrometer equipped with a ^{1}H/^{15}N/^{19}F probe and *z*-axis gradients. Selective ^{19}F irradiation was achieved with a continuous wave at a power level of 40 dB applied over the 1 s recycle delay and the solvent signal was minimized with water flip-back pulses. The spectra were acquired as five interleaved ^{1}H,^{15}N-HSQC experiments with defined selective irradiation frequencies of −131, −138, −141, and −145 ppm and one at an off-resonance position. Proton chemical shifts were referenced relative to internal DSS at 0.0 ppm. ^{15}N, ^{13}C, and ^{19}F chemical shifts were calculated indirectly using the following gyromagnetic ratios: ^{15}N/^{1}H = 0.101329118, ^{13}C/^{1}H = 0.251449530, and ^{19}F/^{1}H = 0.940940080. All spectra were recorded at 25 °C. The NMR chemical shifts have been deposited in the BioMagResBank, www.bmrb.wisc.edu, accession code 15467.

Acknowledgment. This research was supported by the Biotechnology and Biological Sciences Research Council.

JA078000N

(25) Reed, M. A. C.; Hounslow, A. M.; Sze, K. H.; Barsukov, I. G.; Hosszu, L. L. P.; Clarke, A. R.; Craven, C. J.; Waltho, J. P. *J. Mol. Biol.* **2003**, *330*, 1189−1201.